This article is published as part of the *CrystEngComm* themed issue entitled:

Crystal Engineering and Crystallography in the Pharmaceutical Industry

Guest Editors Magali Hickey, Örn Almarsson and Matt Peterson

Published in issue 7, 2012 of *CrystEngComm*

Articles in this issue include:

CrystEngComm

Dynamic Article Links

Cite this: *CrystEngComm*, 2012, **14**, 2404

www.rsc.org/crystengcomm

PAPER

Microfluidic approach to polymorph screening through antisolvent crystallization†

Michael R. Thorson,[a] Sachit Goyal,[a] Yuchuan Gong,*[b] Geoff G. Z. Zhang[b] and Paul J. A. Kenis*[a]

Received 8th September 2011, Accepted 15th December 2011
DOI: 10.1039/c2ce06167h

Here we present a microfluidic platform comprised of 48 wells to screen for polymorphs of active pharmaceutical ingredients (API) through antisolvent crystallization. API solutions and anti-solvents are precisely metered in various volumetric ratios (range from 50 : 10 to 10 : 50), and mixed *via* diffusive mixing on-chip. Optical microscopy and Raman spectroscopy were used to analyze the resultant solids. The small volumes (37 nL) and the ability to screen a wide range of supersaturations through diffusive mixing make this platform especially useful for solid form development at discovery and early development stages in pharmaceutical industry. To validate this microfluidic approach, we conducted on-chip antisolvent crystallization using indomethacin. Solvent choice, supersaturation level, and antisolvent-to-solution ratio were found to affect the resulting crystal form of the solids prepared on chip. We modelled the representative time-dependent concentration profiles during the mixing of the antisolvent and API solutions. Combining this analysis with solubility data yielded spatiotemporal supersaturation profiles, which we correlated with solid formation as observed experimentally.

Introduction

Many efforts in the pharmaceutical industry focus on identifying and controlling polymorphism of active pharmaceutical ingredients (API).[1] Each polymorph has its unique set of thermal, surface, mechanical and other properties, which affect its suitability for a marketed drug.[2–7] Identifying as many available polymorphs as possible allows the selection of a solid form with the best combination of physical properties for product development. In addition, successful solid form screening helps strengthen intellectual property of both final products as well as manufacturing processes.[2] On the contrary, failure to find a polymorph of an API, especially the thermodynamically most stable one, may be costly.[8,9]

This study presents a microfluidic approach to assist in polymorph identification. Polymorph identification requires extensive screening of multiple parameters as no model exists to predict all available polymorphs.[3,10,11] The small scale inherent to microfluidics combined with the ability to mix combinatorially has led to the development of very-large-scale-integration (VLSI) microfluidic devices, which enable the screening of many conditions with limited material.[12–14] VLSI microfluidic platforms have been developed for a wide range of applications including crystallization,[12,15–18] biological detection,[19] DNA sequencing[20] and drug sorting.[21] Specifically, two highly integrated free interface diffusion (FID) platforms have been developed for the crystallization of proteins[12] and salts of APIs.[22] Additionally, microfluidic droplet based systems,[16,18] SlipChip,[17] and selectively functionalized surface devices[15] have been developed for crystallization of proteins and small molecules. To date, however, most microfluidic crystallization efforts have been limited to the applications involving aqueous solutions due to incompatibility of PDMS-based chips with many solvents, including those that are often used for API crystallization.

Here we present a microfluidic chip for polymorph screening of APIs *via* antisolvent crystallization. The compatibility of the chip with a number of organic solvents (here: methanol, ethanol, isopropanol, and DMSO) is improved by reducing the thickness of PDMS layers and adding glass impermeable layers. The chip uses a minimal amount of API to screen an array of solvents and antisolvent-to-solution volumetric ratios. The resulting solids can be characterized on-chip using Raman spectroscopy. We validated the chip by screening for polymorphs of a known API: indomethacin.

Experimental section

Chip assembly

The crystallization platform is comprised of a thin multilayer polydimethylsiloxane (PDMS, General Electric RTV 650 Part A/B) chip fabricated using standard multilayer soft lithographic procedures reported previously[23,24] with some modifications. The thickness of the control layer was reduced to 70 μm by spin

[a]*Department of Chemical & Biomolecular Engineering, University of Illinois at Urbana-Champaign, USA. E-mail: kenis@illinois.edu*
[b]*Materials Science, Global Pharmaceutical R & D, Abbott Laboratories, North Chicago, USA. E-mail: yuchuan.gong@abbott.com*
† Electronic supplementary information (ESI) available. See DOI: 10.1039/c2ce06167h

coating the PDMS (50 : 10 = A:B) at 1300 rpm. Next, the control layer was bonded to a PDMS frame (a 2.5″ square PDMS slab with a 2″ by 1″ window in the center) *via* baking at 60 °C for 30 min, to provide rigidity and allow for transfer of the control layer. Once bonded, 2 mL of hexane was poured onto the control layer, which caused the thin PDMS control layer to swell and separate from the silicon wafer. Then, the control layer was rinsed with water to remove residual hexane, dried, aligned and placed on the fluid layer. The resulting assembly was baked at 60 °C for 30 min to induce irreversible bonding. Solvent impermeable Crystal Clear Tape (Hampton HR4-511) was adhered to the top of the assembled control and fluid layers. Pre-cleaned microscope slides (Fischer Scientific 12-550-A3) were coated with a 20-nm layer of chromium for adhesion, followed by deposition of a 200-nm layer of gold using an E-beam evaporation system (Temescal six pocket E-Beam Evaporation System). Finally, the fluid and control layer assembly was placed on the Au-coated glass substrate. Multiple schematics of the device are provided in the Supplementary Information, Figure S1.

API solution preparation

Indomethacin, and all solvents were obtained from Sigma-Aldrich and used as received. The indomethacin solutions were prepared at 15 mg ml^{-1} in methanol, ethanol, isopropanol, and at 1 g mL^{-1} in DMSO by dissolving 30 mg of powder in its respective solvent in glass vials with mixing (Maxi Mix II, Barnstead/Thermolyne).

Filling of the microfluidic chip and mixing of the solutions

All solutions used on-chip were introduced by first placing 1-2 μL droplets of the API solutions and antisolvent at their respective inlet ports, then, pulling the fluids into the chip *via* actuation of the appropriate valve sets and applying gentle suction at the appropriate fluid outlets. Once the chip was filled, adjacent API solutions and antisolvents were mixed diffusively for 20 min. Throughout the mixing period, the wells were monitored for solid formation using an upright stereo zoom microscope (Leica Z16 APO) equipped with a macro lens (Leica 10447176), a digital camera (Leica DFC280), and a motorized X-Y stage (Semprex KL66). Images of each well were acquired roughly 30 min after initialization of mixing by moving the motorized stage in an automated fashion from well-to-well using Image Pro Plus (Media Cybernetics).

Crystallization off-chip

An antisolvent, water, was added to ethanol, methanol, isopropanol, or DMSO solutions of indomethacin in 1-mL glass vials (Kimmble/Chase) at 8 volumetric ratios (10 : 50, 16 : 44, 21 : 39, 27 : 33, 33 : 27, 39 : 21, 44 : 16, and 50 : 10) such that the total volume was 0.9 mL. The resulting solids in the vials were analyzed *via* birefringence 1 h after mixing.

Solid form analysis

The crystallinity of the solid forms in the wells on-chip was verified *via* birefringence (chips without gold coating on the glass substrate) using a stereo zoom microscope (Leica Z16 APO). In addition, Raman spectroscopy (Renishaw mircoPL/Raman microscope) was used to identify polymorphic forms of indomethacin on-chip (chips with gold coating on the glass substrate). The Raman spectrometer equipped with a 785 nm excitation source (Renishaw NIR 100 mW diode laser) was combined to an upright microscope (Leica DM2500M). Individual wells were centered under a 5× objective in brightfield mode. Raman spectra of individual crystals was collected in the range of 400–1750 cm^{-1} by focusing the laser bean to a spot size of ~5 μm at higher magnification (50×).

Raman spectra identification

Indomethacin solids prepared on-chip were identified by comparing their Raman spectra to the published references. Specifically, amorphous, α, and γ forms of indomethacin exhibit distinct Raman signal, corresponding to the C=O stretch, at 1681 cm^{-1}, 1692 cm^{-1}, and 1698 cm^{-1}, respectively. In addition, the α polymorph exhibits a unique hydrogen bonded acid C=O stretch at 1680 and 1649 cm^{-1}.[25]

Modeling

We simulated the change of concentration profiles throughout the diffusive mixing process of an API solution and an antisolvent using a 2D finite elements solver (FEMLAB 4.2 from COMSOL, Stockholm, Sweden). We used a simplified version of Fick's law to model diffusion of the API as a dilute species:

$$\frac{\partial C_1}{\partial t} + \nabla \cdot (-D_1 \nabla C_1) = 0$$

To accurately model the diffusion of methanol and water, a more complete version of Fick's law was used to account for the change of the fluid density during mixing:

$$\rho \frac{\partial \omega_i}{\partial t} + \nabla \cdot \left(- \left(\rho D_1 \nabla \omega_1 + \rho \omega_1 D_1 \frac{\nabla M_n}{M_n} \right) \right) = 0$$

The density of solution[26,27] and the mutual diffusion coefficients[28] were both interpolated as piecewise cubic functions of methanol concentration. Additionally, the average mass was taken as the molecular weight, M_n. The model was used to determine the concentration profile of the mixture at 1, 5, 10, 25, 40, 100, 250, 500, and 1200 s. Complete mixing was found to be achieved in 1200 s after the onset of mixing. Further details of the model can be found in the Supplementary Information.

Solubility estimation

To calculate supersaturation profiles for indomethacin (see below), we estimated the solubility of indomethacin experimentally as the solubility data of indomethacin in a binary solution of methanol and water was not available in the literature. Indomethacin was added to five, 20-mL glass vials (Kimmble/Chase). Mixtures of methanol and water (methanol to water volumetric ratios of 10 : 1, 8 : 2, 7 : 3, 6 : 4, and 5 : 5) were pipetted into glass vials with an incremental volume of 0.5 ml, 2 ml, or 5 ml depending on the total volume of the added solvent. Following each incremental addition of solvent, the mixture was sonicated

for 1 min and subsequently, visually inspected for the presence of solids. The solubility was calculated based on the total mass of the solid and the total volume of solvent added to the vial. The solubility was fit to the Jouyban-Acree model[29] ($J_0 = -379$, $J_1 = 602$, and $J_2 = 0$) *via* minimization of the square of the errors between the model and the measured solubilities using the Solver add-in in excel.

Calculating supersaturation profiles

Supersaturation is defined as the ratio of actual concentration to solubility.[30] The supersaturation levels were calculated from concentration profiles simulated in the model and solubility data:

$$S(t, x) = \frac{C_{API}(t, x)}{C_{sat}(x_{solvent})} \quad (1)$$

where $S(t, x)$ is the supersaturation level at time t and position x, $C_{API}(t, x)$ is the concentration of the API, and $C_{sat}(x_{solvent})$ is the solubility of indomethacin in the solvent mixture, x_{solvent}. Both the concentration and the solubility of indomethacin are time and position dependent due to the change of solvent composition during continuous mixing.

The solubility of indomethacin in a solvent mixture of water and methanol was calculated using Jouyban-Acree model:[29]

$$\log C_{sat,m,T} = f_1 \log X_{1,T} + f_2 \log X_{2,T} + \frac{J_0 f_1 f_2}{T} + \frac{J_1 f_1 f_2 (f_1 - f_2)}{T} + \frac{J_2 f_1 f_2 (f_1 - f_2)^2}{T} \quad (2)$$

where $C_{\text{sat,m,T.}}$ is the solubility of the API in mixture, m, at the absolute temperature, T; f denotes the fraction of each solvent, 1 and 2, in the mixtures in the absence of the solute, J are the model terms (determined experimentally, see above).

Results and discussion

Design and operation of microfluidic platform

The microfluidic platform is designed to allow precise control *via* a diffusive mixing process, which may increase the chance of crystallization using the antisolvent method.

Chip design. The microfluidic platforms used in this study, which were fabricated and assembled using standard soft lithography procedures, are comprised of an array of 6 × 8 individual 'wells'. A 'well' is defined as a set of two adjacent chambers for an API solution and an antisolvent (Fig. 1). The chambers are filled with API solutions and antisolvents by actuation of pneumatic filling valves as described in previous reports.[31,32] Adjacent sets of API solutions and antisolvents are mixed *via* free interface diffusion upon actuation of the mixing valves (Fig. 1). The volume of adjacent sets of compartments is gradually varied, enabling screening of different antisolvent-to-solution ratios, as schematically shown in a 3 × 3 array in Fig. 1. Specifically, in the 48-well chip used here, eight antisolvent-to-solution ratios (50 : 10 to 10 : 50) were screened in 37-nL wells (combined volume of API solution and antisolvent chambers) for six different combinations of API solutions and antisolvents.

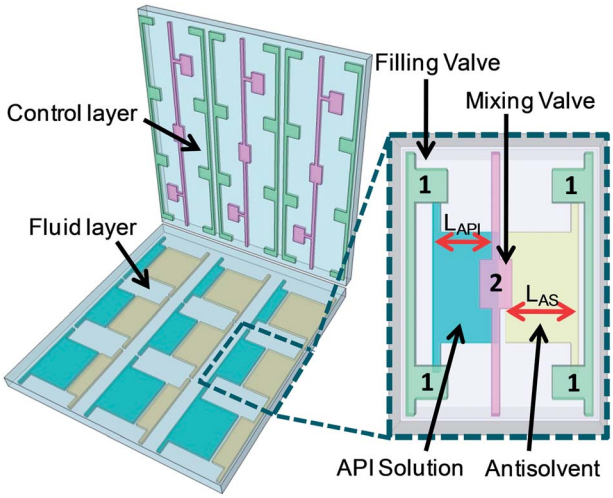

Fig. 1 A schematic depiction of a 3 × 3 array of wells for on-chip antisolvent crystallization. All API solutions (blue) and antisolvent (yellow) solutions are contained in the fluid layer. Each column can contain an API solution at a different concentration and/or in a different solvent. The inset shows an individual well. The antisolvent-to-solution ratio for each well is controlled by varying the L_{API}-to-L_{AS} ratio of the adjacent API solution and antisolvent chambers across the chip. Fluid routing and mixing is achieved using normally-closed pneumatic valves embedded in the control layer. Valve set 1 controls the filling of the columns of solution chambers and valve set 2 allows for mixing of the API solution and antisolvent in adjacent chambers *via* diffusion.

Compared to a traditional screening approach (~900 μl per condition), this constitutes a reduction in volume greater than 20,000 ×. Varying the relative size of the API solution and antisolvent chambers, as expressed in the length of the chambers (L_{API} and L_{AS}, Fig. 1), changes both the final composition and the supersaturation profiles within each 'well'. The dimensions were chosen such that the solutions mixed in roughly 20 min.

Chip operation. This chip reported here operates in a similar fashion to a platform we developed earlier for salt screening.[22] Filling and mixing is controlled *via* the operation of arrays of normally closed (NC) valves.[31–33] NC valves were chosen based on their ability to be integrated at a high density with excellent isolation between adjacent chambers. In addition, the NC valves are closed in rest, which makes the resulting chips highly portable because the chips do not have to be connected continuously to a peripheral pressure source. For filling, 1–2 μL droplets of all API solutions and antisolvents were placed at designated inlet ports with a pipette. Then, the fluid was pulled into the chip *via* actuation of valve set 1 (Fig. 1) and gentle suction at the appropriate fluid outlets. Next, actuation of valve set 2 initiated diffusive mixing between adjacent API solutions and antisolvents. Filling and mixing is further highlighted in Figure S2 in the Supplementary Information.

Solvent compatibility. The PDMS-based microfluidic platform is known to be compatible with a variety of solvents, including those used in this study. However, PDMS may absorb the solvents used in this study (up to 9% increase in PDMS volume due to swelling for these solvents) and these solvents may evaporate through the PDMS layer of a traditional PDMS-based

microfluidic chip.[34] This solvent loss impedes control over the generation and maintenance of supersaturation levels within the chip. We reduced the thickness of the PDMS layer in the chip presented here to minimize solvent absorption. In addition, impermeable layers (Crystal Clear tape and glass) were applied at the top and bottom of the chip to eliminate evaporation. These changes drastically reduced the solvent loss and improved the compatibility of the chip with many organic solvents, including methanol, ethanol, isopropanol, and DMSO. Thus, on-chip crystallization and subsequent analysis over a period of up to 4 h becomes feasible. Among the 38 solvents Lee *et al.* tested, DMSO, 1-propanol, ethanol, and methanol were ranked 19, 21, 24, and 28, respectively, with increasing compatibility to PDMS.[22] We believe that the platform reported in this study would be compatible to the other solvents in the range. The application of the platform in presence of the solvent proved to be less compatible with PDMS (*e.g.*, Acetone, THF) may require an alternative material.

Raman compatibility. Several analytical techniques such as X-Ray, IR, and Raman can be used for crystal form identification.[15,25,35] Raman spectroscopy was used for *on-chip* polymorph identification due to the weak Raman sorption of the thin PDMS layers and the high spatial resolution of the technique. The glass slide at the bottom of the chip was covered with a reflective gold coating to minimize fluorescence from glass on-chip.

Antisolvent crystallization

Indomethacin is known to have several polymorphs, and their crystallization conditions have been published previously.[25,36] Antisolvent crystallization of indomethacin was performed to validate the application of the microfluidic chip in pharmaceutical solid form screening. Methanol, ethanol, isopropanol, and dimethyl sulfoxide (DMSO) solutions of indomethacin were mixed with water (antisolvent) in a 48-well chip (Fig. 2). The wells were monitored for crystal formation using a bright field microscope. Raman spectra of the solids of indomethacin (Fig. 3) prepared on-chip were collected and compared with spectra from literature.[25] For comparison purposes, crystallization of indomethacin was also performed off-chip in 1-mL vials using the same solvents, concentrations, and antisolvent-to-solution ratios.

Table 1 summarizes the solid forms of indomethacin observed both on-chip as well as off-chip in 1-mL vials. Three solid forms of indomethacin were observed on-chip: amorphous, α polymorph, and γ polymorph. The success rate of on-chip crystallization was found to be 63%, slightly higher than that of off-chip crystallization, which was 54%. However, while amorphous solids were observed in a large fraction of the conditions screened off-chip (81% of the conditions screened off-chip compared to 38% on-chip), crystals with high crystallinity were normally obtained on-chip. The higher success rate of crystallization using the microfluidic approach can be attributed to the lower local supersaturation levels during the on-chip crystallization experiment, which resulted from gradual diffusive mixing.

The impact of supersaturation level on the success rate of crystallization was observed in both on-chip and off-chip crystallizations. When water was added to DMSO solution of indomethacin, indomethacin remained in solution at and below antisolvent-to-solution ratios of 16 : 44, but precipitated as amorphous solid at higher antisolvent-to-solution ratios. Indomethacin also precipitated as amorphous solid from methanol solution on-chip when water was added with a ratio of 27 : 33 or higher. However, indomethacin crystallized as α polymorph at lower antisolvent-to-solution ratios. Similar results were obtained in off-chip experiments.

When mixing an ethanol solution of indomethacin with water off chip, we did not observe precipitation at the lowest antisolvent-to-solution ratio of 10 : 50. At higher antisolvent-to-solution ratios, indomethacin crystallized as γ polymorph along with appreciable amount of amorphous content. When the antisolvent-to-solution ratio was increased to 50 : 10, indomethacin precipitated as amorphous solid. On-chip crystallization led to γ form with high crystallinity at all antisolvent-to-solution ratios, except at 50 : 10 when amorphous solid appeared. The comparison of the results of on-chip and off-chip crystallizations suggests that a microfluidic approach could increase the success rate of crystallization.

Specific polymorph of a chemical compounds may be crystallized by selecting crystallization solvents. In the off-chip crystallization experiment described here, indomethacin crystallized as α form in methanol, and γ form in ethanol and IPA. A similar result was obtained in on-chip crystallization, which suggests that the microfluidic platform can be used in finding various polymorphs of an API. The minimum sample requirement gives this approach an advantage in that the study may be conducted at an early stage of drug development with limited sample availability.

It is interesting to note that crystallization of indomethacin behaved differently in isopropanol when it was performed off-chip as compared to on-chip. Crystallized off-chip, only γ polymorph of indomethacin was observed at an antisolvent-to-solution ratio of 21 : 39. However, when the ratio was increased to 27 : 33, α polymorph of indomethacin, a metastable form, was observed. With the antisolvent-to-solution ratio further increased, amorphous indomethacin precipitated, till at 50 : 10 when α polymorph was completed replaced by amorphous solid. The appearance of metastable solid forms in off-chip crystallization may be caused by rapidly reaching high level of local supersaturation (less than a second) following simple turbulent mixing. Comparatively, indomethacin crystallized only as γ polymorph, the thermodynamically most stable form at the room temperature, when it was crystallized on-chip at all antisolvent-to-solution ratios. The selective crystallization of the thermodynamically most stable polymorph on-chip may be due to the slow diffusive mixing at the nL-scale in the microfluidic approach. Supersaturation level gradually increases upon diffusive mixing, which gives a better chance for the thermodynamically stable form to nucleate. Therefore, crystallization using the microfluidic chip may improve the chance of finding the thermodynamically most stable form of pharmaceutical solids.

Relating crystallization outcomes to modeled supersaturation profiles

The nature of the solids prepared in antisolvent crystallization experiments depends on many factors, including solvent type,

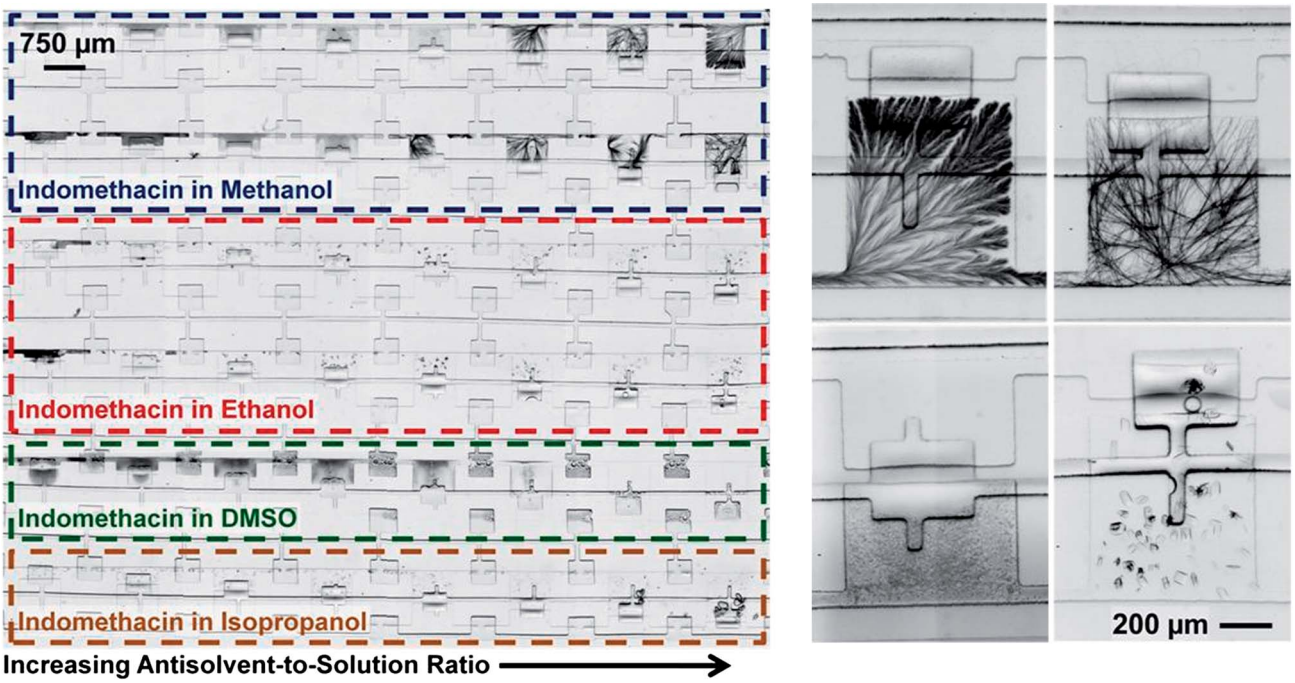

Fig. 2 Optical micrograph of a microfluidic chip after mixing methanol, ethanol, DMSO, and isopropanol solutions of indomethacin with water as the antisolvent. The occurrence of different solids depends on the solvents and the antisolvent-to-solution ratios used. The image on the right shows various indomethacin solid forms grown on-chip.

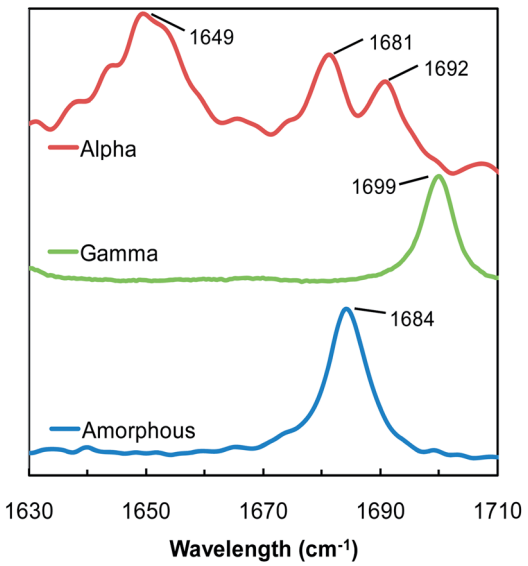

Fig. 3 On-chip Raman spectra of α and γ polymorph, and amorphous indomethacin in 1630 to 1710 cm^{-1} range.

antisolvent-to-solution ratio, and the method of mixing. To explain the difference in the on-chip and off-chip crystallization results, we used a two-dimensional finite-element-method solver (COMSOL) to model the mixing of API solutions and antisolvents *via* counter diffusion in chambers of the same dimensions as those used in the experiments reported above. We used the resulting concentration profiles to obtain supersaturation profiles, and correlated those with the crystallization outcomes.

The model developed here has the potential for a much broader application than what was explore here, for on-chip and off-chip comparison. Specifically, its prediction of time dependent supersaturation profiles can be correlated to spatiotemporal nucleation events. Such a correlation could facilitate the study of kinetic data for crystallization. Specifically, this model could be coupled with other microfluidic diffusive mixing processes[12,17,22] to facilitate kinetic studies. Furthermore, acquisition of kinetic data could aid in the scale-up to the macroscale. However, it is important to realize that different crystallization outcomes may be observed on-chip as compared to the macroscale due to the small sample volumes on-chip, which require higher supersaturations levels for nucleation.

Indomethacin is a poorly water-soluble compound, but has high solubility in many organic solvents, such as methanol, ethanol, and DMSO. Fig. 4a shows the calculated solubility of indomethacin in a methanol/water mixture. The solubility of indomethacin was found to increase slightly when up to ~60% of water was replaced by methanol. However, further replacing water with methanol increases the solubility of indomethacin significantly.

We extracted concentration profiles at different times after the onset of mixing along the center line that connects the API solution chamber and antisolvent chamber at 50% of the chamber height, as indicated in Fig. 4b. The position "0" on the *x*-axis corresponds to the wall of the API solution chamber, whereas position "1" corresponds to the wall of the antisolvent chamber. The initial concentration of indomethacin was high in the API solution chamber, and zero in the antisolvent chamber (Fig. 4c). After the mixing was initiated, the diffusion of indomethacin decreases its concentration in the API solution

Table 1 Polymorphic data for indomethacin solids formed on-chip and off-chip[a]

		Volumetric Ratio of Antisolvent-to-API solution (on-chip/off-chip)							
Solvent[b]		50 : 10	44 : 16	39 : 21	33 : 27	27 : 33	21 : 39	16 : 44	10 : 50
MeOH	1	a[a]/a	a/a	a/a	a/a	a/a,α[a]	α/a,α	α/a,α	a/a,α
	2	a/a	a/a	a/a	a/a	α/a,α	α/a,α	α/a,α	α/a,α
EtOH	1	a,γ[a]/a	γ/a,γ	γ/a,γ	γ/a,γ	γ/a,γ	γ/a,γ	γ/a,γ	γ/-[a]
	2	a,γ/a	γ/a,γ	γ/a,γ	γ/a,γ	γ/a,γ	γ/a,γ	γ/a,γ	γ/-
DMSO		a/a	a/a	a/a	a/a	a/a	a/a	-/-	-/-
IPA		γ/a,γ	γ/a,γ,α	γ/a,γ,α	γ/γ,α	γ/γ,α	γ/γ	γ/-	γ/-

[a] "a" indicates an amorphous solid; "α" and "γ" indicate α and γ polymorphs, respectively; "-" indicates no precipitation. [b] MeOH indicates methanol; EtOH indicates ethanol; DMSO indicates dimethyl sulfoxide; and IPA indicates isopropanol.

chamber and increases its concentration in the antisolvent chamber. Upon complete mixing, equilibrium is reached, and the concentrations of indomethacin in both chambers are equal. During mixing, methanol and water also counter-diffuse into the opposite chamber (Fig. 4d). Before the mixing is completed, the solvent composition is different at each location in the chambers. Thus, the solubility of indomethacin at each location evolves with mixing (Fig. 4e). The modeled concentration profile of indomethacin was found to reach equilibrium slower than both the solvents and the corresponding solubility profile, because the diffusivity of indomethacin is lower than that of the solvents. The spatiotemporal supersaturation levels were calculated using the concentration profile of indomethacin and the solubility profiles at different times following initiation of mixing (Fig. 4f).

It was also noted that the model did not take into consideration depletion of supersaturation level due to the crystallization or precipitation of API. The calculated supersaturation profile at times after crystallization or precipitation may not represent accurately the experimental condition in the chambers. Therefore, only the initial evolution of supersaturation levels following the onset of mixing were used to correlate with the experimental outcome.

Fig. 5 shows experimental outcomes following the mixing of ethanol or methanol solutions of indomethacin (15 mg mL^{-1}) with water at eight different antisolvent-to-solution ratios. The simulated supersaturation profiles corresponding to the experiment conducted in methanol are used to compare with the experimental outcomes side by side. The simulated supersaturation profiles in ethanol/water mixture are believed to be indifferent due to the similar solubility and diffusivity of indomethacin in both solvents.

Immediately following opening the valve, the solubility of indomethacin dropped significantly at the interface of the two solutions due to the fast mixing of methanol and water. However, the concentration of the API solution remained high at the valve due the slower diffusion of indomethacin. Therefore, the supersaturation profile exhibits a sharp peak at the valve representing a high level of supersaturation. Since the concentration of indomethacin, and the diffusivities of methanol and water were same for all of the tested conditions, the modeled supersaturation profiles were independent of the L_{AS}-to-L_{API} ratios immediately after the onset of the mixing.

Spatiotemporal supersaturation levels in the API chamber. Following the onset of mixing, the supersaturation profiles in the API chambers evolved differently for various antisolvent-to-solution ratios:

High antisolvent-to-solution ratios. The supersaturation level in the API solution chamber increased initially, and then, gradually decreased when the two solvents were further mixed. The solubility of indomethacin in methanol decreases significantly with slight increase in water content (Fig. 4a). Soon after mixing, a small amount of water diffusing into the API solution chamber significantly lowered the solubility of indomethacin. Concurrently, indomethacin remained highly concentrated in the API chamber due to its low diffusivity. The combination of high concentration and low solubility of indomethacin in the API solution chamber caused an overshoot of supersaturation levels early in the mixing process such that a maximum supersaturation was reached. Following an "overshoot" of the supersaturation levels, further addition of water to the API chambers had less of an effect on the solubility of indomethacin in methanol (Fig. 4a) but the concentration of indomethacin in the API chambers continued to drop as the API diffused out of the API chambers. The effects associated with the depletion of indomethacin were greater than effects from a decrease in solubility. As a result, the supersaturation levels gradually decreased and reached equilibrium at a lower supersaturation level.

Low antisolvent-to-solution ratios. A similar change in the spatiotemporal supersaturation levels was observed close to the mixing valve. Diffusion of water into the API solution became the rate limiting step of equilibrium for these conditions. Indomethacin and methanol reached equilibrium more quickly than water due to the shorter distance (small antisolvent chamber *vs.* large API solution chamber) to diffuse. The concentration of indomethacin remained unchanged while water diffused to the farther side of API solution chamber. Therefore, the supersaturation level in the API solution chambers increased gradually as water decreased the solubility of indomethacin.

The modeled supersaturation profiles agree with the experimental outcome. Crystallization of indomethacin was observed at low antisolvent-to-solution ratios, such as L_{AS}-to-L_{API} = 10 : 50. The higher crystallization tendency at these conditions can be explained by the gradual increase of supersaturation ratio at lower levels, which gives the API enough time to nucleate. In contrast, indomethacin precipitated mainly as amorphous solids, at high antisolvent-to-solution ratios, such as

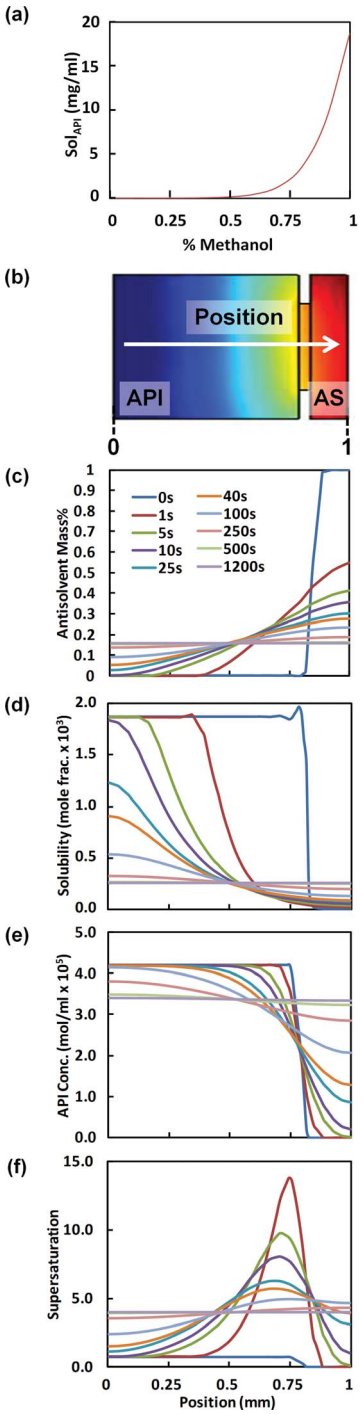

Fig. 4 (a) Calculated solubility of indomethacin in a methanol/water mixture. (b) Schematic depiction of a modeled 'well' where API solution (left) is mixed with antisolvent (right). The farther side of the API solution chamber and the antisolvent chamber is defined as position 0 and 1, respectively. (c) Modeled concentration profile which evolves with mixing. (d) Mass fraction of antisolvent at various positions of the well following mixing. (e) Solubility of indomethacin in the solvent mixture at various positions and times following mixing. (f) Spatiotemporal supersaturation profiles throughout the mixing process.

L_{AS}-to-L_{API} = 50 : 10. This is most likely due to the rapid increase of supersaturation to high levels, which caused API to crash out as amorphous solid immediately following the opening of the valve. Because the crystals which formed on-chip were experimentally observed to have formed before the final supersaturation levels were achieved (<5 min), we believe that spatiotemporal supersaturation profile development plays a significant role in crystal formation.

Spatiotemporal supersaturation levels in the antisolvent chamber. Following the onset of mixing, the supersaturation profiles in the antisolvent chambers also evolved differently for various antisolvent-to-solution ratios:

High antisolvent-to-solution ratios. The solubility of indomethacin increased gradually in the antisolvent chambers when the antisolvent-to-solution ratio was high. The gradual increase in supersaturation levels can be explained by the lower diffusivity of indomethacin as compared to the solvents employed and the larger distance for the API to travel at high antisolvent-to-solution ratios. At these conditions, the diffusion of indomethacin became the rate limiting step. Therefore, the supersaturation level in the antisolvent chambers increased gradually until equilibrium was reached.

Low antisolvent-to-solution ratios. In contrast, indomethacin had a short distance to travel at low antisolvent-to-solution ratios. In addition, there was large amount of indomethacin available to be redistributed into the antisolvent chamber. As a result, the supersaturation level increased rapidly to a high level, and then gradually decreased, due to the depletion of water in the antisolvent chamber, until the mixing was complete.

We did not observe precipitation or crystallization in the antisolvent chambers although supersaturation was obtained based on the model. We believe that precipitation or crystallization occurred in the API solution chambers shortly after the onset of mixing (when the concentration of indomethacin was high in the API chamber) and before equilibrium was reached at all antisolvent-to-solution ratios. Precipitation or crystallization of indomethacin retained a significant amount of indomethacin that was, otherwise, available to diffuse into the antisolvent chambers as predicted by the model. This disturbance prevented precipitation or crystallization of indomethacin in the antisolvent chambers.

Final supersaturation levels. We also observed an interesting trend regarding the final supersaturation levels predicted by the model. As the antisolvent-to-solution ratio became larger, the supersaturation levels increased rapidly until at a ratio of 39 : 21, beyond which, the rate of increase of the final supersaturation levels slowed down. This phenomenon can be explained by the different initial concentration of API and the solubility of indomethacin in the final mixture.

At the lowest antisolvent-to-solution ratios, the supersaturation levels were low due to the high solubility of indomethacin in the final mixture containing a large amount of methanol and a small amount of water even though large amount of indomethacin was present in the chambers. When the antisolvent-to-solution ratio was increased from 10 : 50 to 39 : 21, the amount

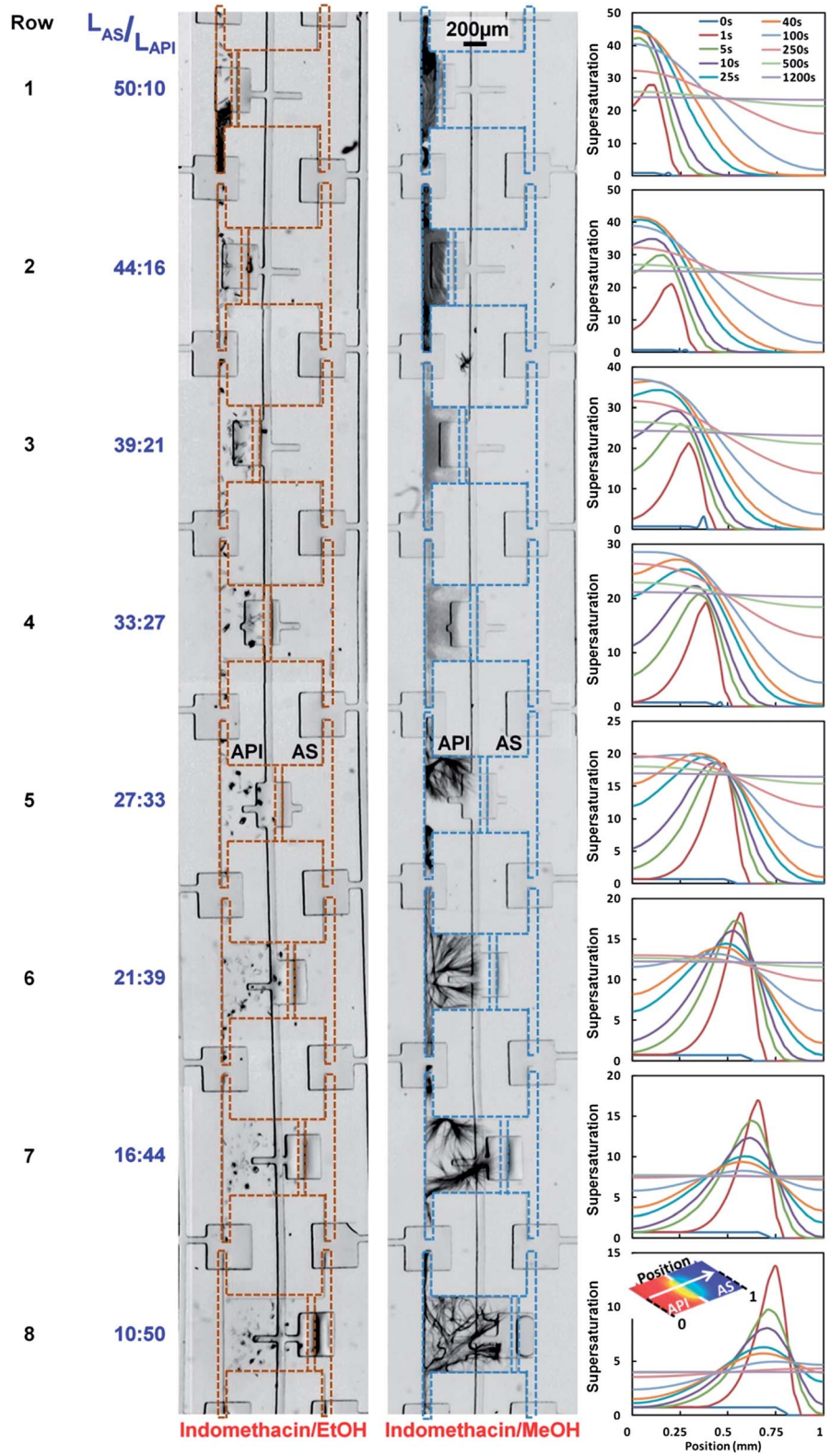

Fig. 5 Correlation of experimental outcomes of the on-chip crystallization of indomethacin with modeled supersaturation profiles (graphs on the right) at eight antisolvent-to-solution ratios (L_{AS}:L_{API}). The experimental data shown here corresponds to rows 2 and 3 in Table 1.

of indomethacin in the chambers decreased proportional to the size of the API solution chamber. The same change in anti-solvent-to-solution ratio reduced the solubility of indomethacin more because water suppresses the solubility of indomethacin more effectively in methanol-rich solvents, Therefore, the final supersaturation level for the mixture increased significantly. The

increase of the final supersaturation level slowed down when antisolvent-to-solution ratios were further elevated by increasing the ration between the size of antisolvent chamber and the API solution chamber to 50 : 10. This is because adding more water to a methanol/water mixture with high water content does not significantly further reduce the solubility, while the indomethacin concentration still decreases proportionally to the size of API solution chamber.

Conclusions

We developed a microfluidic platform for polymorph screening of pharmaceutical active ingredients through antisolvent crystallization. The platform can meter and mix various antisolvent and API solutions in 48 unique conditions. API solutions and antisolvents are mixed on-chip gradually by diffusion, which creates better-controlled supersaturation levels favoring crystallization of API. The platform only requires a total of 37 nL of solution at each crystallization condition, which represents a 20,000× reduction of sample size compared to the conventional automated solid form screening platforms (~900 μl per condition). The small sample size requirement allows solid form screening to be conducted at an early stage of drug development.

The microfluidic platform was validated by the crystallization of indomethacin in methanol, ethanol, isopropanol, and DMSO. The platform was found to enhance the chance of crystallization comparing to the conventional antisolvent crystallization. In general, crystalline solids exhibited better crystallinity at lower antisolvent-to-solution ratios. In addition, both α, and γ forms of indomethacin were prepared through on-chip crystallization.

We modeled the evolving supersaturation profiles during on-chip diffusive mixing. The supersaturation profiles were calculated using the concentration and solubility of indomethacin at various locations and times following the onset of mixing. The calculated supersaturation profiles were well correlated to the crystallization outcomes. We concluded that the better crystallization tendency using microfluidic platform is due to the slow increase of supersaturation levels, especially to a relatively lower level.

The microfluidic platform developed here may find its application in crystallization design at macro level. Crystallization can be conducted at wide range of conditions in a single chip with controlled diffusive mixing. Correlation among nucleation time, nucleation location in the chamber, and the calculated supersaturation profile may allow us to better define a design space for crystallization scale-up.

Furthermore, the modeling showed that high supersaturations are formed at the mixing interface. As a result, the platform could be further modified so as to decrease the rate of change of supersaturation at the interface. The chamber geometries and/or concentrations could be modified to make the mixing process more gradual.

Acknowledgements

We would like to thank Abbott Laboratories for financial support. Part of this work made use of the facilities in the Micro- & Nanotechnology Laboratory as well as the Frederick Seitz Materials Research Laboratory Central Facilities at University of Illinois at Urbana-Champaign, which are partially supported by the U.S. Department of Energy under grants DE-FG02-07ER46453 and DE-FG02-07ER46471. We also would like to acknowledge Amit Desai for stimulating discussions.

Notes and references

1 G. H. Brittain, *Polymorphism in Pharmaceutical Solids*, M. Dekker, New York, 1999.
2 A. R. Liberski, G. J. Tizzard and J. J. Diaz-Mochon, *et al.*, *J. Comb. Chem.*, 2008, **10**, 24–27.
3 S. L. Morissette, Ö. Almarsson and M. L. Peterson, *et al.*, *Adv. Drug Delivery Rev.*, 2004, **56**, 275–300.
4 S. M. Berge, L. D. Bighley and D. C. Monkhouse, *J. Pharm. Sci.*, 1977, **66**, 1–19.
5 C. R. Gardner, O. Almarsson and H. Chen, *et al.*, *Comput. Chem. Eng.*, 2004, **28**, 943–953.
6 R. Krishna, *Applications of pharmacokinetic principles in drug development*, Kluwer Academic/Plenum Publishers, 2004.
7 L. X. Yu, M. S. Furness and A. Raw, *et al.*, *Pharm. Res.*, 2003, **20**, 531–536.
8 P. Jain and A. K. Banga, *Int. J. Pharm.*, 2010, **394**, 68–74.
9 J. Bauer, S. Spanton and R. Henry, *et al.*, *Pharm. Res.*, 2001, **18**, 859–866.
10 M. L. Peterson, S. L. Morissette and C. McNulty, *et al.*, *J. Am. Chem. Soc.*, 2002, **124**, 10958–10959.
11 C. P. Price, A. L. Grzesiak and A. J. Matzger, *J. Am. Chem. Soc.*, 2005, **127**, 5512–5517.
12 C. L. Hansen, E. Skordalakes and J. M. Berger, *et al.*, *Proc. Natl. Acad. Sci. U. S. A.*, 2002, **99**, 16531–16536.
13 T. Thorsen, S. J. Maerkl and S. R. Quake, *Science*, 2002, **298**, 580–584.
14 M. C. Cole, A. V. Desai and P. J. A. Kenis, *Sens. Actuators, B*, 2011, **151**, 384–393.
15 A. Y. Lee, I. S. Lee and S. S. Dette, *et al.*, *J. Am. Chem. Soc.*, 2005, **127**, 14982–14983.
16 P. Laval, C. Giroux and J. Leng, *et al.*, *J. Cryst. Growth*, 2008, **310**, 3121–3124.
17 L. Li, W. Du and R. F. Ismagilov, *J. Am. Chem. Soc.*, 2009, **132**, 112–119.
18 B. Zheng, L. S. Roach and R. F. Ismagilov, *J. Am. Chem. Soc.*, 2003, **125**, 11170–11171.
19 B. R. Schudel, M. Tanyeri and A. Mukherjee, *et al.*, *Lab Chip*, 2011, **11**, 1916–1923.
20 R. G. Blazej, P. Kumaresan and R. A. Mathies, *Proc. Natl. Acad. Sci. U. S. A.*, 2006, **103**, 7240–7245.
21 C. B. Rohde, F. Zeng and R. Gonzalez-Rubio, *et al.*, *Proc. Natl. Acad. Sci. U. S. A.*, 2007, **104**, 13891–13895.
22 M. R. Thorson, S. Goyal, B. R. Schudel, *et al.*, *Submitted*, 2011.
23 C. L. Hansen, E. Skordalakes and J. M. Berger, *et al.*, *Proc. Natl. Acad. Sci. U. S. A.*, 2002, **99**, 16531–16536.
24 M. A. Unger, H. P. Chou and T. Thorsen, *et al.*, *Science*, 2000, **288**, 113–116.
25 L. S. Taylor and G. Zografi, *Pharm. Res.*, 1997, **14**, 1691–1698.
26 N. A. Lange and J. A. Dean, *Lange's Handbook of chemistry*, McGraw-Hill, 1979.
27 D. R. Lide, *CRC handbook of chemistry and physics: a ready-reference book of chemical and physical data*, CRC Press, 2005.
28 Z. J. Derlacki, A. J. Easteal and A. V. J. Edge, *et al.*, *J. Phys. Chem.*, 1985, **89**, 5318–5322.
29 A. Jouyban, *Handbook of Solubility Data for Pharmaceuticals*, CRC Press, Boca Raton, 2010.
30 S. Talreja, P. J. A. Kenis and C. F. Zukoski, *Langmuir*, 2007, **23**, 4516–4522.
31 B. R. Schudel, C. J. Choi and B. T. Cunningham, *et al.*, *Lab Chip*, 2009, **9**, 1676–1680.
32 R. Mohan, B. R. Schudel and A. V. Desai, *et al.*, *Sens. Actuators, B*, 2011, **160**, 1216–1223.
33 W. H. Grover, A. M. Skelley and C. Liu, *et al.*, *Sens. Actuators, B*, 2003, **89**, 315–323.
34 J. N. Lee, C. Park and G. M. Whitesides, *Anal. Chem.*, 2003, **75**, 6544–6554.
35 Y. Meng, D. J. Weidner and G. D. Gwanmesia, *et al.*, *J. Geophys. Res.*, 1993, **98**, 22199–22207.
36 A. Heinz, M. Savolainen and T. Rades, *et al.*, *Eur. J. Pharm. Sci.*, 2007, **32**, 182–192.

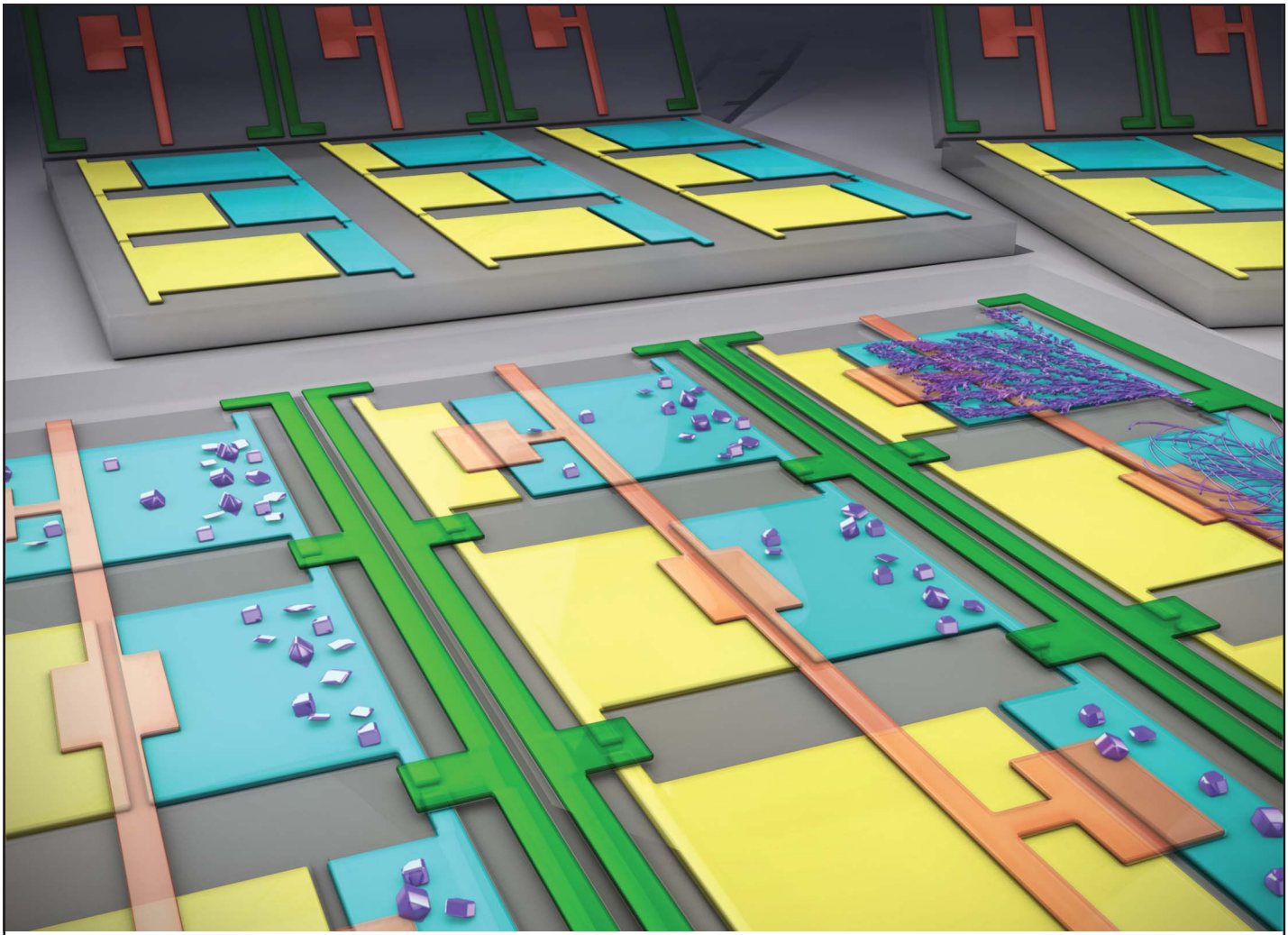

Showcasing research from the Paul J. A. Kenis laboratory, University of Illinois at Urbana-Champaign.

Title: Microfluidic approach to polymorph screening through antisolvent crystallization

Combinatorial screening for polymorphism and crystal habit of pharmaceuticals using a microfluidic platform comprised of an array of 37-nanoliter wells.

Image credits: Mike Thorson, Jeremy Miller, Ryan Durdle, Alex Jerez of ITG, Beckman Institute.

As featured in:

See Thorson, Goyal, Gong, Zhang and Kenis, *CrystEngComm*, 2012, **14**, 2404.

RSC Publishing

www.rsc.org/crystengcomm

Registered Charity Number 207890